Biomedical Optics EXPRESS

Laser speckle contrast imaging with extended depth of field for *in-vivo* tissue imaging

Iliya Sigal,[1,2] Raanan Gad,[1,2] Antonio M. Caravaca-Aguirre,[3] Yaaseen Atchia,[1,2] Donald B. Conkey,[3] Rafael Piestun,[3] and Ofer Levi[1,2,*]

[1]*The Edward S. Rogers Sr. Department of Electrical and Computer Engineering, 10 King's College Road, Toronto, ON M5S 3G4, Canada*

[2]*Institute of Biomaterials and Biomedical Engineering, University of Toronto, 164 College Street, Toronto, ON M5S 3G9, Canada*

[3]*Department of Electrical, Computer, and Energy Engineering, University of Colorado at Boulder, Boulder, UCB 425, CO 80309, USA*

[*]*ofer.levi@utoronto.ca*

Abstract: This work presents, to our knowledge, the first demonstration of the Laser Speckle Contrast Imaging (LSCI) technique with extended depth of field (DOF). We employ wavefront coding on the detected beam to gain quantitative information on flow speeds through a DOF extended two-fold compared to the traditional system. We characterize the system *in-vitro* using controlled microfluidic experiments, and apply it *in-vivo* to imaging the somatosensory cortex of a rat, showing improved ability to image flow in a larger number of vessels simultaneously.

OCIS codes: (110.6150) Speckle imaging; (110.7348) Wavefront encoding; (170.6480) Spectroscopy, speckle

References and links

1. A. K. Dunn, H. Bolay, M. A. Moskowitz, and D. A. Boas, "Dynamic imaging of cerebral blood flow using laser speckle," J. Cerebral Blood Flow Metab. **21**, 195–201 (2001).
2. D. A. Boas and A. K. Dunn, "Laser speckle contrast imaging in biomedical optics," J. Biomed. Opt. **15**, 011109 (2010).
3. J. D. Briers and S. Webster, "Laser speckle contrast analysis (lasca): a nonscanning, full-field technique for monitoring capillary blood flow," J. Biomed. Opt. **1**, 174–179 (1996).
4. M. Draijer, E. Hondebrink, T. Leeuwen, and W. Steenbergen, "Review of laser speckle contrast techniques for visualizing tissue perfusion," Lasers in Medical Science **24**, 639–651 (2009).
5. A. Fercher and J. Briers, "Flow visualization by means of single-exposure speckle photography," Opt. Comm. **37**, 326–330 (1981).
6. Y. Atchia, H. Levy, S. Dufour, and O. Levi, "Rapid multiexposure in vivo brain imaging system using vertical cavity surface emitting lasers as a light source," Appl. Opt. **52**, C64–C71 (2013).
7. D. D. Duncan and S. J. Kirkpatrick, "Can laser speckle flowmetry be made a quantitative tool?" J. Opt. Soc. Am. A **25**, 2088–2094 (2008).
8. S. Yuan, A. Devor, D. A. Boas, and A. K. Dunn, "Determination of optimal exposure time for imaging of blood flow changes with laser speckle contrast imaging," Appl. Opt. **44**, 1823–1830 (2005).
9. H. Levy, D. Ringuette, and O. Levi, "Rapid monitoring of cerebral ischemia dynamics using laser-based optical imaging of blood oxygenation and flow," Biomed. Opt. Express **3**, 777–791 (2012).
10. Y. Atchia, H. Levy, S. Dufour, and O. Levi, "Speckle contrast at deviations from best focus in microfluidic and in vivo," in Biomedical Optics and 3-D Imaging, (Optical Society of America, 2012), p. BTu3A.49.
11. W. T. Cathey and E. R. Dowski, "New paradigm for imaging systems," Appl. Opt. **41**, 6080–6092 (2002).
12. E. R. Dowski, W. T. Cathey, and S. C. Bradburn, "Aberration invariant optical/digital incoherent systems," Optical Review **3**, A429–A432 (1996).

#199179 - $15.00 USD Received 9 Oct 2013; revised 27 Nov 2013; accepted 27 Nov 2013; published 6 Dec 2013

13. Q. Yang, L. Liu, and J. Sun, "Optimized phase pupil masks for extended depth of field," Opt. Comm. **272**, 56–66 (2007).
14. Y. Takahashi and S. Komatsu, "Optimized free-form phase mask for extension of depth of field in wavefront-coded imaging," Opt. Lett. **33**, 1515–1517 (2008).
15. R. C. Gonzalez and R. E. Woods, *Digital Image Processing*, 3rd ed. (Prentice-Hall, Inc., Upper Saddle River, NJ, USA, 2006).
16. J. Breckinridge, D. Voelz, and J. B. Breckinridge, *Computational Fourier Optics: A MATLAB Tutorial*, Tutorial Text Series (SPIE Press, 2011).
17. J. W. Goodman, "Some fundamental properties of speckle," J. Opt. Soc. Am. **66**, 1145–1150 (1976).
18. B. Forster, D. Van De Ville, J. Berent, D. Sage, and M. Unser, "Complex wavelets for extended depth-of-field: A new method for the fusion of multichannel microscopy images," Microscopy Res. Technique **65**, 33–42 (2004).
19. T. B. Rice, S. D. Konecky, A. Mazhar, D. J. Cuccia, A. J. Durkin, B. Choi, and B. J. Tromberg, "Quantitative determination of dynamical properties using coherent spatial frequency domain imaging," J. Opt. Soc. Am. A **28**, 2108–2114 (2011).
20. T. B. Rice, S. D. Konecky, C. Owen, B. Choi, and B. J. Tromberg, "Determination of the effect of source intensity profile on speckle contrast using coherent spatial frequency domain imaging," Biomed. Opt. Express **3**, 1340–1349 (2012).
21. G. Grover, S. Quirin, C. Fiedler, and R. Piestun, "Photon efficient double-helix psf microscopy with application to 3d photo-activation localization imaging," Biomed. Opt. Express **2**, 3010–3020 (2011).
22. P. Miao, H. Lu, Q. Liu, Y. Li, and S. Tong, "Laser speckle contrast imaging of cerebral blood flow in freely moving animals," J. Biomed. Opt. **16**, 090502 (2011).
23. D. B. Conkey, A. M. Caravaca-Aguirre, and R. Piestun, "High-speed scattering medium characterization with application to focusing light through turbid media," Opt. Express **20**, 1733–1740 (2012).
24. S. Quirin and R. Piestun, "Depth estimation and image recovery using broadband, incoherent illumination with engineered point spread functions," Appl. Opt. **52**, A367–A376 (2013).

1. Introduction

Laser speckle contrast imaging (LSCI) is an established imaging modality for measuring relative flow speeds of scattering particles such as red blood cells [1]. The modality was adopted by the biomedical optics community for its ability to measure blood flow in superficial tissue, such as exposed brain cortex or skin, in wide-field [2–4]. The technique involves illuminating a region of interest of a scattering sample with coherent light, and capturing the resulting random interference pattern using a camera. When no movement takes place in the field of view (FOV), the resulting image is a static stochastic interference pattern called speckle, seen as a random distribution of bright and dark pixels. In regions of the FOV where movement is present the speckles appear blurry compared to their static counterparts, and the amount of blur is related to the speed of scatterers in that location. It is possible to quantify relative velocities of scatterers by computing the speckle contrast in a small neighbourhood around a pixel as follows [5]:

$$K = \frac{\sigma(I)}{\langle I \rangle} = \sqrt{\frac{\tau_c}{2T}\left[1 - \exp\left(\frac{-2T}{\tau_c}\right)\right]}. \tag{1}$$

In the above equation, K is the local speckle contrast, $\sigma(I)$ is the standard deviation of the recorded intensity around a single pixel, $\langle I \rangle$ is the mean intensity around that pixel, T is the camera exposure time, and τ_c is the speckle decorrelation time defined as $\tau_c = 1/ak_0\bar{v}$, where a is a scatterer-dependent proportionality constant, k_0 is the wavenumber of light, and $\bar{v}$ is the mean velocity of scatterers. Such formulation allows for a simple relationship to be obtained between the speckle contrast and the flow speeds when $T \gg \tau_c$: $K \propto 1/\sqrt{\bar{v}}$. This limit is known as the "long exposure limit". As such, we refer to the quantity $1/K^2$ as the "flow index" or "relative flow speed", as it is linearly proportional to the absolute flow speed. We note that Eq. (1) assumes a Lorentzian distribution of scatterers; the use of a Gaussian distribution model does not result in appreciably different outcomes in practice [6].

While the LSCI technique is very simple to implement, care needs to be taken in quantitatively interpreting its results. Non-uniform scatterer size will skew the speckle contrast maps to

#199179 - $15.00 USD Received 9 Oct 2013; revised 27 Nov 2013; accepted 27 Nov 2013; published 6 Dec 2013

slower, larger scatterers [7]. In addition, selecting an appropriate camera integration time needs to be optimized per application [8]; short exposure times deviate from the convenient linear relationship between the flow index and the flow speeds, while longer exposure times accumulate error due to sensitivity to motion artefacts in the system. In many cases, calibration against another technique, such as time-of-flight [9] allows for reliable quantitative LSCI studies. Our previous work also explored the limitation of the technique to provide reliable quantitative information when the moving scatterers are not located in the plane of best focus of the imaging system [10], and found that misfocus leads to an underestimate of the flow velocities in blood vessels. Misfocus-induced errors present a challenge in applying the technique to wide-field *in-vivo* imaging. For example, when using LSCI to measure blood flow speeds in rodent brains, a craniotomy is typically performed to expose the brain tissue. The surgical procedure inevitably causes an inflammatory response that leads to brain swelling, which results in the brain surface forming a meniscus rather than a plane. In such case, there will inevitably be vessels above and below the imaging system's focal plane. Using a smaller aperture-stop size in the imaging system will result in a larger FOV in focus, however this approach has two key limitations. First, reducing the aperture size significantly reduces the amount of light collected, requiring longer exposure times to avoid the increase in camera shot noise. Secondly, lowering the numerical aperture (NA) of the imaging system increases the size of the individual speckles [2], and results in lower spatial resolution. In this work we increase the depth of field (DOF) of the LSCI system while keeping the numerical aperture of the system at its highest value.

Wavefront coding is a technique that can be used to extend the DOF of an imaging system that has been initially conceived and characterized for incoherent imaging [11]. The technique involves placing a phase mask in the imaging system in order to make the point spread function (PSF) of the system become less sensitive to misfocus. Such a PSF distorts the image at best focus and from adjacent planes, however the distorted PSF changes little between the adjacent planes compared to a traditional system. This makes the imaging system shift invariant with defocus, which allows restoring image fidelity using a deconvolution. In this work we evaluate the use of wavefront coding as means to extend the depth of field of the LSCI technique, and demonstrate the ability to measure flow speeds in a larger number of blood vessels compared to the traditional system, *in-vivo*.

This paper is organized as follows: section 2 further introduces the wavefront coding technique, and describes our imaging system. Section 3 presents the numerical and experimental characterization results. Section 4 discusses the advantages and limitations of our proposed technique, while section 5 concludes the work.

2. Optical imaging system

Wavefront coding, in most general terms, is a technique to alter the wavefronts' propagation in an incoherent imaging system using a tailored phase mask, for a desired application. For example, an application could be either extending the DOF [11] or reducing optical aberrations [12]. We seek to implement this approach to extend the DOF of the LSCI technique, which uses coherent light.

Following the methodology described in [11] we impose a phase mask of the following form on the detected light path:

$$\phi(x,y) = \frac{2\pi}{\lambda}\alpha\left(x^3+y^3\right), \tag{2}$$

where x and y are the spatial coordinates in the plane perpendicular to the beam path, λ is the wavelength of light, and α is a proportionality constant with units of m^{-2}. The constant α determines the "strength" of the imposed phase, whereby a greater benefit in DOF extension is

#199179 - $15.00 USD Received 9 Oct 2013; revised 27 Nov 2013; accepted 27 Nov 2013; published 6 Dec 2013

expected for higher values of α, with the trade-off being lower signal-to-noise ratio (SNR) due to distortion-induced overlap of neighbouring speckles and features. The cubic phase function is a member of the set of functions that will result in PSF that is invariant to defocusing; a substantial body of work has been done on phase function optimization, and the interested reader is referred to references [13] and [14]. We used the well-characterized cubic phase function in this proof-of-concept work, while acknowledging that further phase function optimization for our system should yield better system performance.

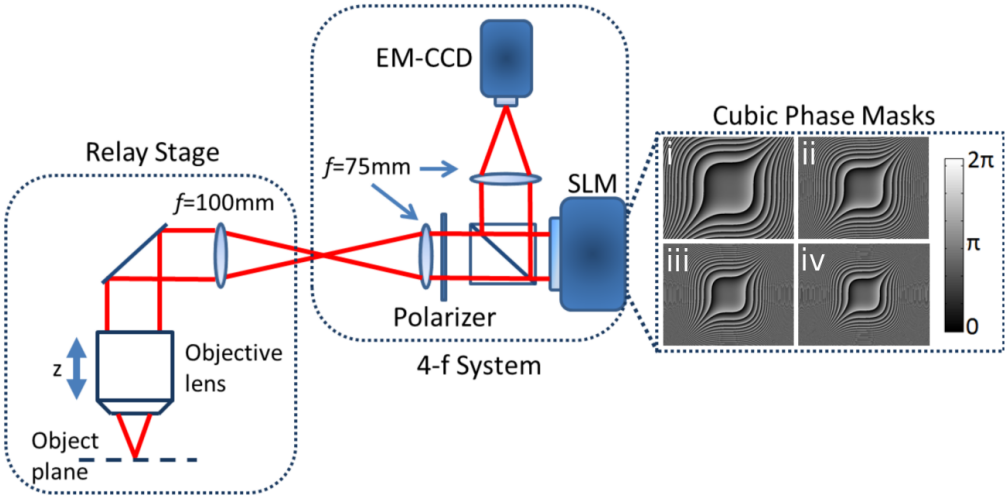

Fig. 1. Schematic of the experimental setup. The setup consists of two stages: a relay stage and a 4-f imaging stage. The relay stage is used to set the magnification of the system and translate the object plane that is parallel to the optical table to an intermediate image plane that is parallel to the SLM surface. The objective is mounted on a translation stage with μm-resolution. The unit-magnification 4-f imaging stage contains an SLM placed in the Fourier plane. The SLM is used to impose a cubic phase mask on the incoming beam. Sample phase masks are shown in the right-hand side of the figure: i) α = 23 m^{-2}, ii) α =35 m^{-2}, iii) α = 47 m^{-2}, iv) α = 58 m^{-2}

Figure 1 shows a schematic of the imaging system used. The core of the system is a 4-f lens configuration with a spatial light modulator (LCOS-SLM, Hamamatsu Photonics, Hamamatsu City, Japan) placed in the Fourier plane. The SLM imposes the cubic phase mask on the detected beam. The right-hand side of Fig. 1 illustrates the different phase masks that are imposed on the detected beam. A relay imaging system, employing a $f = 40$ mm, NA=0.14 objective lens (Motic Plan Apo ELWD, WD=34 mm) and a $f = 100$ mm achromatic doublet field-lens, was used to create a 2.5× magnification between the object plane and the entrance plane of the 4-f imaging system. The objective lens was mounted on a translation stage (SM1Z, Thorlabs, Newton, New Jersey, USA) allowing μm-resolution translation of the objective with respect to the imaged specimen. A 90-degree mirror was employed to image a surface parallel to the optical table for the practical purpose of imaging a live rat brain. A 14-bit EM-CCD camera (Rolera EM-C^2, QImaging, Surrey, BC, Canada) was used to record the images. A 30 mW HeNe laser was used as a light source for all imaging experiments.

Figure 2 shows the change of the PSF of the traditional (clear aperture) and extended-DOF systems between the plane of best focus and a plane 200 μm away from best focus. The figure illustrates that the PSF due to the induced cubic phase changes significantly less with misfocus compared to the traditional PSF. As such, the system can be treated as shift-invariant with

#199179 - $15.00 USD Received 9 Oct 2013; revised 27 Nov 2013; accepted 27 Nov 2013; published 6 Dec 2013

misfocus (within a range of misfocus values where optical aberrations are small). Furthermore the convolution kernel of an incoherent imaging system has no zeroes in its pass-band, and therefore a deconvolution may be used to restore image fidelity. For coherent imaging, the cubic phase function produces uniform image distortion for a range of misfocus values, just as for incoherent imaging. However, deconvolution cannot be applied directly to the raw images due to the kernel having zeros in its pass band. Since the relative flow velocity maps are phase-independent, they can be seen as incoherent images with an applied blur filter that closely resembles the PSF of the cubic phase mask. Furthermore, the typical contrast values we see range from ~ 0.25 to ~ 0.01, suggesting a degree of partial coherence in the images. Therefore, we propose that a numeric deconvolution of the PSF from the computed relative velocity maps may be applied to restore the maps' fidelity, and the deconvolution kernel in such case may be approximated by the cubic PSF. To obtain the cubic PSF experimentally, we imaged a back-illuminated 10 μm-diameter aperture located at the focal plane of the imaging system, using a red LED as a light source. We apply the deconvolution via a Wiener filter [15, section 5.8], where the noise parameter was selected empirically. We evaluate the validity of our proposition both using qualitative simulations and using controlled flow experiments *in-vitro*.

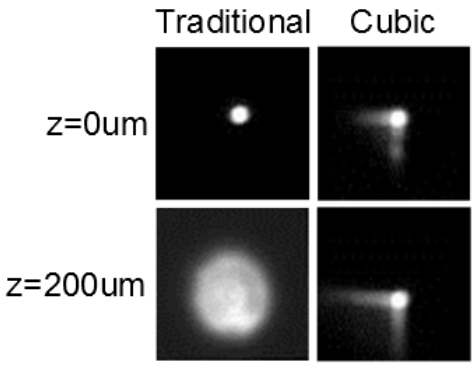

Fig. 2. Point spread function (PSF) change with misfocus for the traditional (left) and extended DOF (right) systems, illustrating the behaviour of the system with misfocus. Images taken were of a 10μm-diameter pinhole illuminated from the back with a red LED, at 5× magnification.

3. Experiments and results

To verify the ability of the cubic phase mask to extend the DOF of the LSCI technique we validate the following: a) the linear relationship between the velocity signal as measured with LSCI and the actual flow velocities holds for physiologically-relevant flow speeds, and b) the relative flow speed values obtained with extended-DOF LSCI vary less with misfocus compared to conventional LSCI. In the following subsections we describe numerical and experiment studies to confirm the above hypotheses.

3.1. Numerical simulations

We simulate the propagation of blurred speckle images through our 4-f imaging system in order to gain insight on the benefits and potential drawbacks of wavefront coding as applied to LSCI. The simulations are performed by propagating speckle patterns using a Fresnel transfer function, similarly to the process outlined in reference [16]. In LSCI employing the long exposure

#199179 - $15.00 USD Received 9 Oct 2013; revised 27 Nov 2013; accepted 27 Nov 2013; published 6 Dec 2013

limit, flow velocity relates to speckle contrast as $\bar{v} \propto 1/\sqrt{K}$. Using the fact that the incoherent superposition of uncorrelated speckle patterns scales as $K = K_0/\sqrt{N}$ [17], where K_0 is the speckle contrast of a single image and N is the number of images incoherently super-imposed, we produce speckle contrast maps with different values of K. Conveniently, N scales linearly with flow velocity: linearly increasing N has the same mathematical effect on the speckle contrast maps as linearly increasing flow speeds. For example, "doubling the flow speed" is akin to adding double the number of uncorrelated speckle patterns. Therefore, we can take N as a measure of the absolute flow speeds in our simulations: to simulate continuously increasing flow in a capillary, we average over continuously increasing N number of different randomly generated speckle patterns.

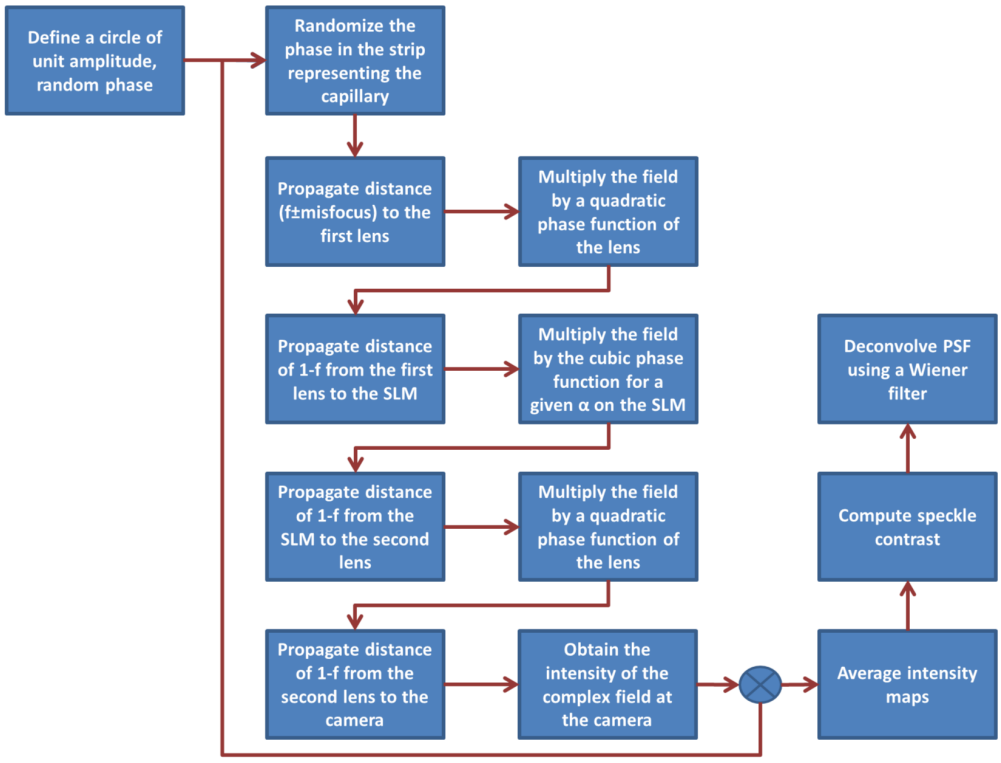

Fig. 3. Flow diagram for the procedure to simulate speckle propagation in our optical system. Free space propagation is performed using the paraxial Fresnel transfer function of free space, similar to a procedure in [16]. The capillary strip is re-randomized N times, and resulting raw speckle intensity images are averaged. Misfocus is simulated by changing the distance between the object plane and the first lens to be different than the focal length of the lens.

The simulation steps are summarized in Fig. 3. The input plane is taken to be a circular aperture surrounded by a stop. The amplitude of the field values in the circle was set to unity and the phase was randomly distributed. We define a "capillary" in the input plane as a strip of pixels in the middle of the plane. To simulate flow of a certain (arbitrary) velocity value, the pixels in the capillary strip in the input plane are re-randomized N different times, and propagated through the system. The raw speckle intensity images are averaged, followed by computation of the LSCI maps and deconvolution of the PSF.

Figure 4 shows both the increase of the DOF and decrease in the velocity range for various

#199179 - $15.00 USD Received 9 Oct 2013; revised 27 Nov 2013; accepted 27 Nov 2013; published 6 Dec 2013

values of α. The DOF is taken as the distance from the location of the objective at best focus to where the integrated flow index across the "capillary" is reduced to 80% of its maximum value. The velocity range is taken as the ratio between the mean relative flow value in the middle of the "capillary" to the "rest" flow value in a region outside of the "capillary". The physical significance of the velocity range is that it is a measure of the SNR.

The results show two trends: DOF increases, while the velocity range decreases, for increasing values of α. The reduction in the velocity range comes due to overlap of point spread functions of adjacent speckles (self-blurring), effectively reducing the contrast corresponding to the "rest" flow velocity.

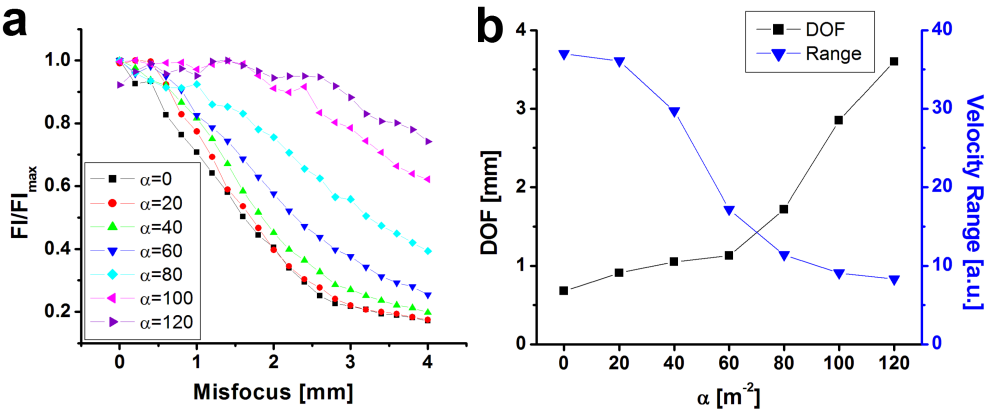

Fig. 4. Results of the numerical simulations. The speckle pattern in the "capillary" was re-randomized $N = 15$ times. Simulations were performed for $N = 5$ and 10 to confirm the linear relation between speckle contrast reduction and N, showing almost identical results. a) Relative change in the flow index with misfocus. α values are in units of m^{-2} b) The DOF and velocity range as a function of α [m^{-2}].

3.2. *in-vitro characterization of extended-DOF LSCI*

We performed controlled *in-vitro* flow experiments to test the linear relationship between the absolute and relative flow speeds. Figure 5 describes the *in-vitro* characterization device, fabricated using a 3D printer, used to explore the effect of imposing a phase mask on the LSCI technique. The device consists of a rectangular "tub" with a series of 400 μm holes defined on two of its sides. The relative placement of holes, and their size, are shown in Fig. 5(b). Hollow glass tubes with an outer diameter of 360 μm and inner diameters varying from 75 μm to 150 μm were placed in the holes, mimicking blood vessels of different diameters at different depths in tissue. The tub was filled to different levels with a scattering gel (1% agarose, 2% dairy cream), mimicking scattering brain tissue. 10% dairy cream was flown inside the capillaries, mimicking blood. A high-precision perfusion pump (Harvard Apparatus Pump 11 Pico Plus Elite) was used to control the flow rate in the capillaries. The measurement arrangement is depicted in Fig. 5(c). Two sets of experiments were carried out: a test to validate linear relationship between relative and absolute flow velocities, and a test to quantify the DOF extension due to imposed phase mask. Every data point in all *in-vitro* experiments represents an average of 100 flow maps in order to minimize the impact of camera noise and transient flow inhomogeneity.

#199179 - $15.00 USD Received 9 Oct 2013; revised 27 Nov 2013; accepted 27 Nov 2013; published 6 Dec 2013

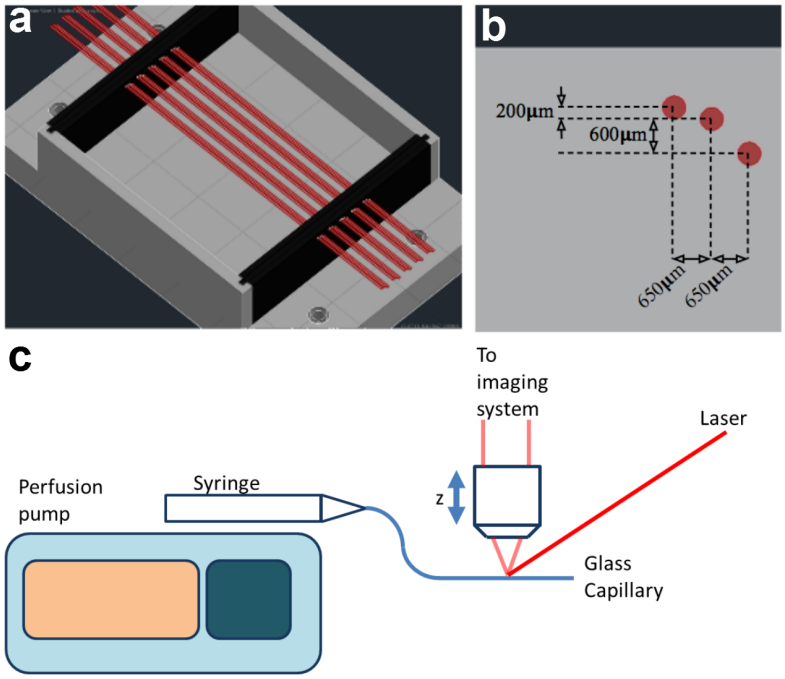

Fig. 5. a) *in-vitro* characterization device: a rectangular tub contains scattering phantom, which can be filled to desired depth, with a holes that fix hollow glass capillaries. Hollow glass tubes with an outer diameter of 360 µm and inner diameters varying from 75 µm to 150 µm were placed in the holes. b) Cross section of the device, showing the size and relative placement of the holes. c) A schematic of the experimental setup. A perfusion pump is used to control the flow rate in a glass capillary, while a HeNe laser is used as a light source.

3.2.1. Impact of wavefront coding on linearity between LSCI-measured and actual flow velocities

This experiment was performed in order to validate whether the flow index remains linear with flow speed for different values of α. No fluid was present in the tub. Coffee cream was perfused in a single capillary with varying pump flow rates, corresponding to varying average speeds. The capillary was placed in the plane of best focus of a traditional imaging system ($\alpha = 0$). The speckle contrast maps were recorded for different values of α.

Figure 6 presents the results of this experiment, showing the dependence of the flow index on the average flow speed for both the traditional system ($\alpha = 0$), and for values of α ranging from 35 m^{-2} to 70 m^{-2}, inside a 75 µm-wide capillary (the line connecting data points is a guide to the eye). The capillary is placed in a plane of best focus of the imaging system. The results confirm the linear relationship between the flow index and the flow speed for the traditional system (black curve), and indicate a deviation from the linear behaviour at higher flow speeds for higher values of α. This suggests that the simple long exposure model for discerning flow from speckle contrast maps holds as long as the distortion that is imposed on the beam is not too strong. Deviations from linearity occur for higher flow rates and higher values of α, indicating that care must be taken in selecting an appropriate phase mask to ensure model validity. Qualitatively, deviation from the model will occur when the distortion creates cross-talk between adjacent speckles. The range of values of α that were tested in the experiments were empirically determined by imaging a de-focused USAF target. Prior to the first reported

#199179 - $15.00 USD Received 9 Oct 2013; revised 27 Nov 2013; accepted 27 Nov 2013; published 6 Dec 2013

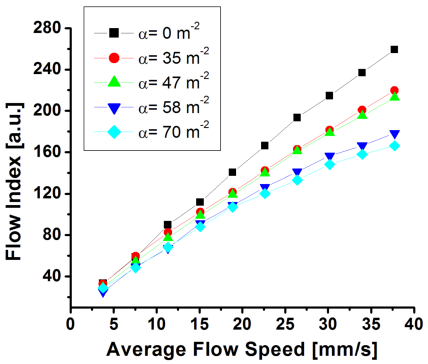

Fig. 6. Maximum flow index vs. average flow speed in a 75 μm-wide capillary, for different values of α. The horizontal axis shows the average flow velocity in the capillary that is set using the perfusion pump. The vertical axis shows the corresponding velocity as measured using LSCI. For traditional LSCI (black squares), the linear relation between the two holds. For extended-DOF LSCI, the linear relation breaks down for higher values of α and higher flow velocities.

data point ($\alpha = 35$ m^{-2}), very little increase in the DOF was empirically observed, and as such it was deemed not critical to image flow for smaller α values. The simulations can provide qualitative insight as to what happens for low values of α, as shown in Fig. 4(b).

3.2.2. Impact of wavefront coding on LSCI DOF extension

To quantify the DOF extension we get from imposing a cubic phase mask we measured the flow maps in a 75 μm-wide capillary while axially translating the microscope objective with respect to the capillary. The focal plane was thus translated from above to below the capillary, while the flow rate remained constant at 32 mm/sec. The speckle contrast maps were recorded at each position of the objective for different values of α. This experiment was performed twice - with the capillary suspended in air, and with the capillary suspended (but not covered in) a phantom.

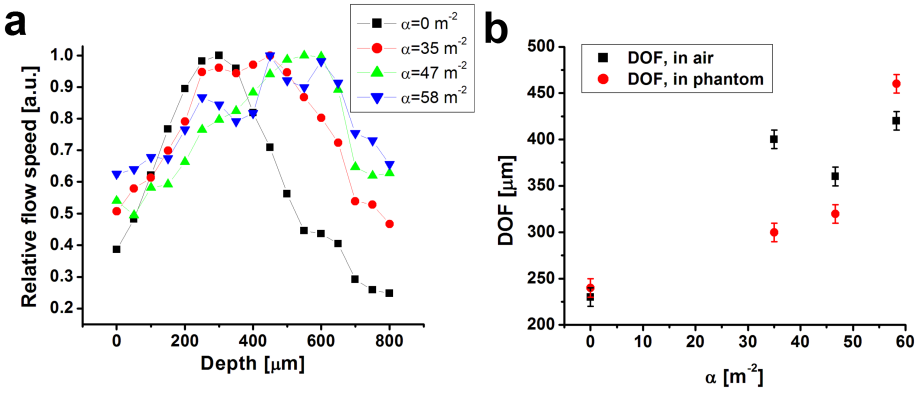

Fig. 7. DOF of the LSCI technique. a) Relative flow speed deviation from its maximum value with misfocus inside a 75 μm-wide capillary, suspended in air. b) DOF, defined as the range of misfocus where the relative flow speed is within 20% of its maximum value, as a function of α, for a capillary immersed in air and in phantom.

#199179 - $15.00 USD Received 9 Oct 2013; revised 27 Nov 2013; accepted 27 Nov 2013; published 6 Dec 2013

Figure 7(a) shows the deviation of the flow index from its maximum value with misfocus, for different values of α. We see a most-rapid decrease in the flow index for the case of $\alpha = 0$ m^{-2} (traditional LSCI), indicating the narrowest DOF. We choose to define the DOF as the region of misfocus where the flow index change is $< 20\%$ of its maximum value, and plot the DOF in Fig. 7(b). The results show that the DOF of the LSCI technique is indeed extended by $\sim$2 using wavefront coding, and the presence of a scattering phantom in proximity to the capillary lowers the extension of the DOF. We propose that the reason for the reduction in the DOF under the presence of the phantom is due to contribution of static speckle from around the flowing fluid. The results also show a fluctuation the LSCI-derived flow values as a function of misfocus for $\alpha = 58$ m^{-2}. We attribute the reason for this the fluctuation to the lower SNR due to phase-mask induced overlap between adjacent speckles.

3.3. Application of extended-DOF LSCI in-vivo

We imaged the somatosensory cortex of a healthy rat through a cranial window in order to demonstrate the benefit of using extended-DOF LSCI to measure brain blood flow speeds *in-vivo*. The imaging study was conducted on an anaesthetized (2-3% isoflurane) male Sprague Dawley rat (approx. 300g), following a surgical protocol described in [6]. The animal study was performed in accordance with ethics protocols approved by the University of Toronto Animal Care Committee.

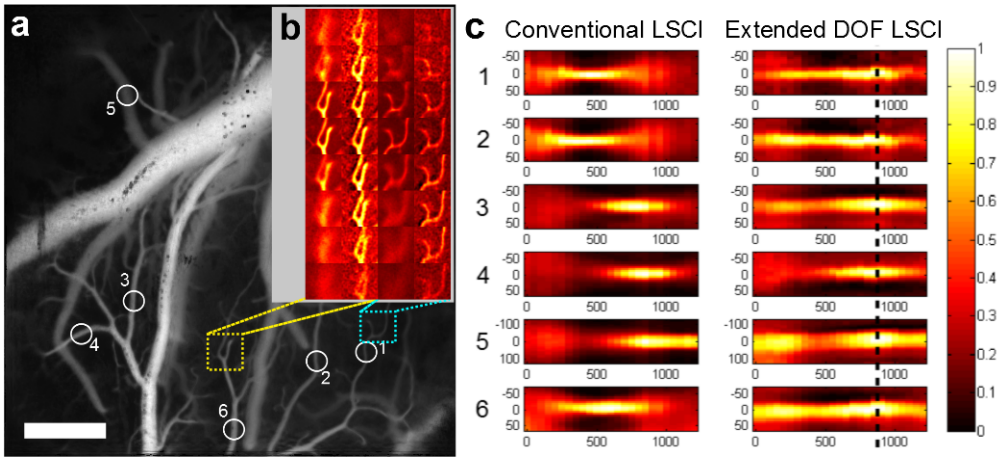

Fig. 8. *in-vivo imaging results*. a) A flow index map of the vasculature, produced using the complex wavelet transform method [18], for illustrative purposes. The vasculature map is an interpolation of traditional LSCI maps taken at different positions of the microscope objective with respect to the brain surface. Scale bar is 400 μm. b) a selection of two regions of vasculature illustrating the effect of the extended-DOF LSCI technique: columns 1 and 3 from the left illustrate the vessels flow index profiles as a function of misfocus for conventional LSCI, while columns 2 and 4 from the left illustrate the vessel flow profiles for extended-DOF LSCI. Consecutive frame are 150 μm apart in misfocus. c) Transverse flow velocity profile for selected vessels in a). The vertical axis is the transverse direction across a vessel, in μm. The horizontal axis is the position of the microscope objective against an arbitrary height above the brain surface ($z = 0$), in μm. The left-hand set of plots pertain to the conventional LSCI technique, while the right-hand set of plots pertain to the extended-DOF LSCI technique where $\alpha = 47$ m^{-2}. These plots were normalized by the maximum velocity in every vessel, where the color map shows the normalized speed. The vertical dashed line indicates a position of the objective where accurate flow information can be read from all selected vessels using the extended-DOF LSCI technique.

#199179 - $15.00 USD Received 9 Oct 2013; revised 27 Nov 2013; accepted 27 Nov 2013; published 6 Dec 2013

The cranial window was illuminated obliquely using a HeNe laser. The objective lens was translated vertically with respect to the cranial window using a micrometer screw, and at every vertical position of the objective 300 images were recorded, for several values of α. The individual speckle contrast maps were computed, and averaged to reduce the impact of shot noise. The relative flow velocity maps were obtained from the contrast maps by taking the squared reciprocal of the contrast value at every pixel. The PSF was deconvolved from the relative flow velocity maps using a Wiener filter.

Several vessels in the FOV were selected (Fig. 8(a)), and the transverse vessel velocity profile was recorded for the different objective lens positions (Fig. 8(c)). For every vessel under consideration, the transverse velocity profile was averaged over a short longitudinal section along the vessel to obtain an average local profile in order to minimize the artefacts due to changes in local concentration of static scatterers, flow inhomogeneities, and other transients that may mask the behaviour of the speckle contrast. The best results (showing a useful DOF improvement with reasonably high SNR as illustrated in Fig. 8(b)) were obtained for $\alpha = 47$ m^{-2}, and all results presented here are for that particular phase mask.

We draw two conclusions from the *in-vivo* imaging results: first, since the region of high relative velocity extends for appreciably larger range of objective lens position for $\alpha = 47$ m^{-2} compared to the traditional system ($\alpha = 0$ m^{-2}), the DOF of the system employing a cubic phase mask is indeed longer. The second conclusion is that the extended DOF system allows selecting a single position of the objective (dashed lines in Fig. 8(c), right hand set of images) where the selected vessels are at their best focus. This is not possible using the traditional LSCI system, as there is no overlap in the maxima of the flow profiles (Fig. 8(c), left-hand set of images). The latter conclusion demonstrates the benefit of using an extended-DOF LSCI system by extracting more reliable quantitative flow information from a larger area across swollen tissue surface, which allows to truly exploit the wide-field benefits of the LSCI technique *in-vivo*.

4. Discussion

In this work we presented an approach to alleviate the sensitivity of the LSCI technique to misfocus. We encoded phase information on the beam to access augmented information on flow speeds. Similar approaches of encoding information on the beam for LSCI have been proposed by Rice et. al. [19, 20], where the spatial frequency domain structured illumination method was extended to the coherent regime as means by which to gain quantitative information on the scattering properties of a material.

We demonstrated that wavefront-coded LSCI fulfils the condition of linearity between relative and absolute flow speeds, provided that the phase distortion imposed on the beam is not too large ($\alpha = 47$ m^{-2} and lower, in our experiments). This implies the ability to use the previously developed model for extracting relative velocity values from speckle maps. We also quantified the increase of the DOF due to the encoded cubic phase mask to be $\sim$2. Since the DOF scales linearly with f-number, a two-fold improvement in the DOF allows us to gain four-fold increase in the photon flux arriving at the camera. Based on our *in-vivo* and *in-vitro* experiments, we can conclude that our proposition to use the incoherent PSF as an approximate deconvolution kernel for LSCI is valid for the imaging parameters we used.

We also found that the cubic phase mask caused a reduction of the speckle contrast due to distortion-induced overlap of adjacent speckles. This led to a decrease (increase) of the static speckle contrast (relative flow speed). In turn, this resulted in a decreased range of relative velocities, as seen both in simulation and in experiment. This reduction in the velocity range typically decreases the SNR. To circumvent this drawback, additional averaging can be used to gain higher accuracy of flow measurements, similar to the procedure in [9]. Doing so will

#199179 - $15.00 USD Received 9 Oct 2013; revised 27 Nov 2013; accepted 27 Nov 2013; published 6 Dec 2013

reduce both temporal resolution and shot noise, and as such, a compromise needs to be reached between the need for measurement accuracy and acquisition speed.

The threshold value for the size of the DOF in this paper was empirically defined as range of vertical positions of the objective yielding flow values that are within 20% of their maxima. Deviations below 10-20% are not easily discernible by eye while trying to estimate the location of best focus during an imaging session. True best focus can be obtained by finely scanning the vertical position of the object plane, and we found that measured flow values at apparent best focus deviate by 10-20% from the values at true best focus. We took the lower end of that range – 20% decrease from maximum – as the boundary of the in-focus region. If we have taken the more stringent 90% (or the less stringent 70%) threshold, the relative maximum improvement we would have measured in the DOF would have been similarly close to two-fold.

We used an SLM to impose a static phase mask in the beam path, which has two drawbacks preventing easy adoption: the high cost of the device, and the need to work in a reflection geometry with normal incidence using just one (horizontal) polarization, leading to light lost. Nonetheless, one could fabricate such phase mask with conventional photolithography techniques [21], and place it in the beam path to extend the DOF. Such mask will be particularly useful to incorporate in a miniature, animal-mounted systems for chronic studies, such as the one reported in [22]. The phase encoding can also be implemented using faster micro-mirror based projector devices, similar to one used in reference [23]. While a key property of such devices – their reconfigurability – is not utilized in the approach proposed here (we envision an approach more akin to placing a prism or a filter in the beam path), there may be applications where the ability to scan through a number of phase masks in rapid succession may be of utility. Another consideration for implementing the technique is the degree of partial coherence in the image: when the speed of scatterers is very high (or exposure time is very long) the coherence is reduced. However, we note that in our in-vivo experiment the lowest speckle contrast recoded was 0.02 in fast arteries, indicating a finite degree of partial coherence. We therefore conclude that loss of coherence in practical terms does not detract from the proposed technique's ability to extend the DOF.

We note that there is a reasonably good agreement between the values of α needed for DOF improvement in simulation and experiment; 2-fold improvement in the DOF is achieved with $\alpha = 80$ m^{-2}, while a similar improvement is achieved with $\alpha = 35 - 47$ m^{-2} in experiment. There are a number of reasons for the discrepancy between the two: first, the simulations do not take into account the oblique nature of the illumination, the true three-dimensional shape of the capillary, or a dynamic scatterer distribution in space that truly represents a blood cell. Secondly, the background contrast values are always lower in experiment due to the finite coherence length of the light source, speckle decorrelation that is induced due to multiple scattering by the tissue, and motion artefacts (primarily heart beat). Thirdly, our naive assumption that number of uncorrelated speckle patterns correspond linearly to speed does not allow for direct predicting ability of our numerical model.

The proposed method uses a deconvolution as a post-processing step, which may be computationally intensive. In this work the deconvolution has been applied in a post-processing step using a built-in MATLAB routine, which takes ≈ 1 second per flow map to complete. Since we performed all our image analysis after the imaging session, speed of computation has not been a major consideration for this proof-of-concept work. For applications that require real-time imaging, open-source software packages such as OpenCV or hardware-based implementations using FPGAs can perform the filtering faster than MATLAB.

The work presented here also opens the door for additional investigation of LSCI and related techniques where phase-encoding helps gain additional information on the nature of the flow, enabling more robust measurements. Future work will involve finding a phase function which

#199179 - $15.00 USD Received 9 Oct 2013; revised 27 Nov 2013; accepted 27 Nov 2013; published 6 Dec 2013

causes less distortion-induced speckle overlap, which will enhance the SNR of the technique. We will also work on developing a more robust method for determining the exact deconvolution kernel to reduce noise due to post-processing. Along similar lines, extending our recent work on using the double-helix PSF in the context of microscopy to LSCI will allow us to obtain information on the axial location of the scattering elements [24], while using the wavefront shaping techniques to impose information on the incoming beam may allow us to improve the limited penetration depth of the LSCI technique [23].

5. Conclusion

In this paper we presented, to our knowledge, a first demonstration of the LSCI technique with extended DOF. The wavefront coding technique was extended to the coherent imaging regime: a cubic phase element was placed in the beam path, thus rendering the PSF of the system to be less sensitive to misfocus. A numerical deconvolution was applied to the computed relative flow velocity maps in a post-processing step to remove the distortion the phase mask imposed on the image. We numerically simulated and experimentally determined the validity of our proposed technique to measure physiologically-relevant flow velocities both *in-vivo* and *in-vitro*. We found that for relatively low-distorting phase the linear relationship between the flow index and the flow velocity holds true for a large range of physiologically-relevant speeds, making the wavefront coding technique a robust means by which to extend the DOF of the LSCI technique. For strongly-distorting phases, the PSF of the neighbouring speckles begin to overlap, which causes a deviation from the linear relation between flow speed and flow index. We demonstrate the application of the extended-DOF LSCI technique during *in-vivo* experiment, showing the ability to select a plane of best focus which provides quantitative information on a larger number of vessels at a given objective position.

Acknowledgement

The authors thank Dr. Suzie Dufour and Dene Ringuette for assistance with animal surgeries, Dmitri Tsvik (RapidProtos Inc.) for assistance in fabricating the microfluidic emulator, Arash Joushaghani for helpful discussions, Christopher Ryan from QImaging for helpful discussions and assistance in fast camera operations, and Dr. Gregory Scholes for loaning the SLM unit. This work was supported in part through the University of Toronto departmental start-up funds to OL, the Natural Sciences and Engineering Research Council of Canada (NSERC) Discovery Grant RGPIN-355623-08 and Collaborative Health Research Project Grant CPG-121050, and by the Networks of Centres of Excellence of Canada, Canadian Institute for Photonic Innovations (CIPI). RG acknowledges partial support through MITACS postdoctoral fellowships; IS acknowledges support through NSERC CREATE: CARE graduate fellowship; YA acknowledges support through NSERC CREATE: MATCH graduate fellowship and the Ontario Graduate Scholarship. We acknowledge support from the National Science Foundation awards DBI-1063407, and DGE-0801680. IGERT: Interdisciplinary Graduate Education in Computational Optical Sensing and Imaging.

#199179 - $15.00 USD Received 9 Oct 2013; revised 27 Nov 2013; accepted 27 Nov 2013; published 6 Dec 2013